THE JOURNAL OF PHYSICAL CHEMISTRY C

Article

pubs.acs.org/JPCC

Alloying and Structure of Ultrathin Gallium Films on the (111) and (110) Surfaces of Palladium

Werner Stadlmayr, Veronika Huber, Simon Penner, Bernhard Klötzer, and Norbert Memmel*

Institute of Physical Chemistry, University of Innsbruck, A-6020 Innsbruck, Austria

Supporting Information

ABSTRACT: Growth, thermal stability, and structure of ultrathin gallium films on Pd(111) and Pd(110) are investigated by low-energy ion scattering and low-energy electron diffraction. Common to both surface orientations are growth of disordered Ga films at coverages of a few monolayers (T = 150 K), onset of alloy formation at low temperatures ($T \approx$ 200 K), and formation of a metastable, mostly disordered 1:1 surface alloy at temperatures around 400−500 K. At higher temperatures a Ga surface fraction of ∼0.3 is slightly stabilized on Pd(111), which we suggest to be related to the formation of Pd_2Ga bulk-like films. While on Pd(110) only a Pd-up/Ga-down buckled surface was observed, an inversion of buckling was observed on Pd(111) upon heating. Similarities and differences to the related Zn/Pd system are discussed.

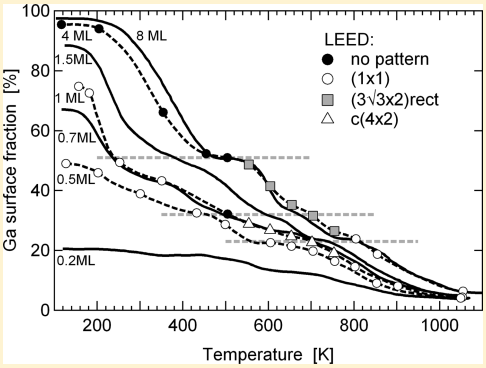

1. INTRODUCTION

CO_2-selective methanol steam reforming (MSR) is one of the most promising reactions to obtain clean hydrogen with low CO content.[1] A number of different catalyst systems are used to facilitate the CO_2-selective reaction, including Cu/ZnO and a class of oxide-supported Pd-based intermetallic compounds, basically comprising PdZn/ZnO, Pd_2Ga/β-Ga_2O_3, and PdIn/bcc-In_2O_3[2−6] In the past decade the latter catalyst groups have been scrutinized in detail, and many aspects of their structural and catalytic properties are already satisfactorily covered. This is especially true for the archetypical Pd−Zn system, where a huge number of different model and supported systems have been studied to result in the clearest picture.[1,6−9] For Pd−Ga, however, some questions regarding the correlation of structural and catalytic properties still remain to be answered. There is common agreement, that a Pd_2Ga intermetallic phase is a prerequisite to obtain high CO_2-selectivities in MSR,[2,5,6,10] although there is strong evidence for a dominating role of the Pd_2Ga/Ga_2O_3 interface, in close correlation to the PdZn/ZnO system.[5,6,10−13] One of the crucial parameters for obtaining high CO_2 selectivities in MSR is efficient water activation, supposedly proceeding fast on either oxide sites close to the intermetallic phase or directly at special interfacial sites. However, especially for Pd−Ga, despite the progress that has been made highlighting the important role of that particular interface, its formation mechanism, and especially its structural prerequisites, remain unclear up to now. Tackling this problem usually requires the use of well-defined model systems. Such model systems in the present case might include near-surface intermetallic phases, prepared either on polycrystalline Pd foils or palladium single crystal surfaces. Both systems have already been shown to be indispensable tools for highlighting the specific structural and/or catalytic peculiarities of the Pd−Zn and Pd−Ga systems.[6,11,13−19] In this respect, surface-science studies of the PdZn near-surface intermetallic phase, formed on Pd(111) and Pd foils, clearly revealed the structural prerequisites for obtaining a high CO_2-selectivity: The latter was only observed, if a distinct Zn-up/Pd-down surface buckling was formed on a PdZn multilayer alloy.[13] The corresponding catalytic experiments of the (as well multilayered) Pd−Ga near-surface intermetallic phase did not yield CO_2-selective states;[11] however, a detailed structural and compositional analysis of PdGa near-surface intermetallic systems is not available so far.

Given the similarities of oxide-supported Pd−Zn and Pd−Ga intermetallic particles in the MSR performance on the one hand and the different behavior of the near-surface bimetallic films on the other hand, we aim at characterizing the structure of the bimetallic Pd−Ga films on Pd substrates. This in turn might provide the basis for understanding, why for PdZn/Pd the supposedly active intermetallic/oxide interface can be formed under MSR reaction conditions, whereas for the corresponding Pd−Ga phase this is not the case. Eventually this will reveal if and under which conditions structural (dis-) similarities, e.g., a "Ga-up/Pd-down" surface corrugation, exist that may be related to the differences in the catalytic behavior of the bimetallic films. To gain full insight into the formation of Pd−Ga intermetallic phases and at the same time to achieve the largest overlap and correlation to other less-defined systems, both the Pd (111) and Pd (110) surface terminations are examined.

Besides the importance of these material combinations as model systems for the investigation of methanol steam

Received: July 24, 2013
Revised: August 30, 2013
Published: September 2, 2013

reforming, we also aim at exploring the similarities and differences of zinc and gallium growth and alloying on both Pd(111) and Pd(110) in order to rationalize the influence of the deposited material as well as of the surface orientation on the formation and structure of the near-surface intermetallic films.

As for Pd−Zn, this goal will be accomplished by studies using a dedicated low-energy ion-scattering (LEIS) setup which, using specific scattering conditions, allows monitoring the top-layer composition. Furthermore, also impact-collision ion scattering spectroscopy (ICISS) measurements were performed, where the backscattering intensity is recorded as a function of the polar or azimuthal angle of incidence of the ion-beam. From these measurements information about surface structure and surface ordering can be obtained by utilizing the shadow-cone concept. For the principles of this technique we refer the reader to various review articles.[20−22] Additional structural information was obtained from low-energy electron diffraction (LEED).

2. EXPERIMENTAL SECTION

All experiments were carried out in an UHV-chamber with a base pressure below 1×10^{-10} mbar. The Pd(111) and Pd(110) crystals were mounted on a 6-axis manipulator with three translational and three rotational degrees of freedom. The sample temperature could be varied between 120 and 1200 K. The palladium surfaces were cleaned by sputtering with 600 eV Ar^+ and annealing to 1000−1150 K. Then the surface was exposed to 7−10 langmuirs of oxygen at $T < 350$ K. The surface was considered to be clean of carbon, if subsequent temperature-programmed desorption (TPD) showed the presence of a clear O_2 desorption peak rather than evolution of CO or CO_2.

As will also be discussed in sections 3 and 4 below, gallium could not be removed from the surface by thermal desorption, but by sputtering only. However, alloy formation and diffusion of Ga atoms into the bulk of the Pd crystals which occurred during the course of the heating experiments led to the formation of a Ga reservoir in the bulk of the substrates that could not be completely removed by sputtering. From these reservoirs, segregation of gallium atoms back to the surface was observed when the surface was annealed during surface preparation in order to heal out the defects created by the argon sputtering. As a consequence, a small Ga signal (approximately 5%) was always present on the surface, even after extensive sputter-anneal cycles.

Gallium was evaporated from a boron-nitride crucible heated by electron-bombardment. An integral flux monitor allowed monitoring the deposition flux. Ga ions created by the electron-impact heating were deflected out of the deposition beam by a negative potential. During deposition the sample was kept at a temperature of 150 K. Ga coverages are quoted in monolayer (ML) equivalents with one monolayer corresponding to the atom density of the respective Pd surface, i.e., 14×10^{14} atoms/cm^2 for Pd(111) and 9.3×10^{14} atoms/cm^2 for Pd(110).

LEIS/ICISS experiments were performed with a differentially pumped ion gun equipped with a Wien filter and an electrostatic hemispherical energy analyzer. All experiments were performed with 5 keV Ne^+ ions at a scattering angle of 160°. Unless otherwise noted, experiments were carried out along the $[\bar{2}11]$ azimuthal direction on Pd(111) and along $[\bar{1}12]$ on Pd(110).[23] To determine the composition of the top-layer exclusively, polar angles of incidence (measured relative to grazing incidence) of $\psi = 45°$ (on Pd(111)) and $\psi = 32°$ (on Pd(110)) were used. In these scattering geometries second-layer atoms are hidden within the shadow cone cast by top layer atoms as long as atoms reside at or close to fcc positions. Hence second layer (and deeper lying) atoms do not contribute to the scattering signal. For recording temperature-induced changes of surface compositions, the samples were heated with a constant rate of 1 K/s while simultaneously monitoring the intensity of the backscattering peaks from Pd and Ga surface atoms, respectively. The relative elemental sensitivity ratio for palladium and gallium was also obtained from these measurements by plotting the intensity of the Ga signal versus that of the Pd signal (Figure 1). As can be seen, all experiments show

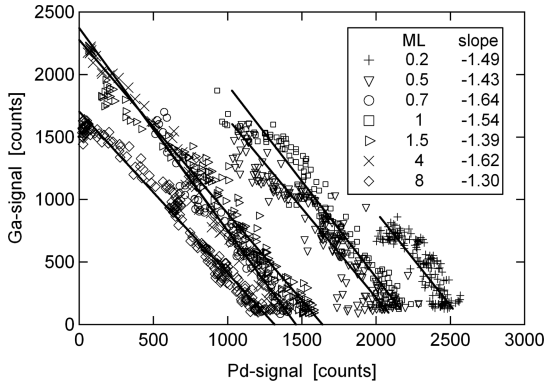

Figure 1. Ga LEIS signal versus Pd LEIS signal measured during annealing of gallium films with various initial coverages. All curves show a similar linear decrease with a weighted average slope of −1.45, indicating a elemental sensitivity ratio $S_{Ga}/S_{Pd} = 1.45$.

an essentially linear behavior, indicating that matrix effects can be neglected. From the average slope of the linear fits an elemental sensitivity ratio $R = S_{Ga}/S_{Pd} = 1.45$ is inferred. This ratio was used to calculate the top-layer concentrations C_{Ga} from the measured intensities I_{Ga} and I_{Pd} as $C_{Ga} = I_{Ga}/(I_{Ga} + RI_{Pd})$

For the structural measurements by LEED or angular ICISS scans, the samples were heated to the targeted temperature with the same heating rate (1 K/s) as in the LEIS experiments described above and then immediately cooled. Measurements were then made at room temperature or below.

3. Ga/Pd(111)

3.1. Growth and Coverage Calibration. In Figure 2 the fraction of gallium in the top-layer as measured by low-energy ion scattering (LEIS) is depicted versus deposition time for a deposition temperature of 150 K. At short deposition times the data points show a steep linear increase. As the Ga surface content increases beyond 60%, the uptake curve levels off and approaches the 100% level only slowly. Hence the Ga films do not exhibit a perfect layer-by-layer growth; rather, at higher coverages, several layers are filled simultaneously, leading to a rough surface morphology. Assuming that initially all deposited atoms reside within the topmost layer, the time for deposition of a monolayer can be estimated from the initial linear increase by extrapolation to a level of 100%. This yields a value of ∼130 s (dashed line in Figure 2). This value was used in the following work for calculating Ga coverages from deposition times.

We would like to note that LEIS in the chosen scattering geometry cannot distinguish between Ga atoms present in a Ga

dx.doi.org/10.1021/jp407337q | J. Phys. Chem. C 2013, 117, 19558−19567

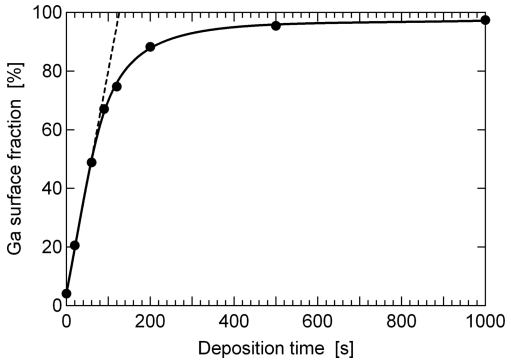

Figure 2. Top-layer gallium content versus deposition time on Pd(111) as obtained from low-energy ion scattering. The deposition temperature was 150 K. The dahed line shows the behavior expected for layer-by-layer growth. The solid line was drawn as a guide to the eye.

adlayer and Ga atoms that have alloyed into the topmost Pd layer (and that are not covered by other atoms). Hence the initial linear intensity increase shown in Figure 2 would also be compatible with such a surface-alloy scenario. In such a case Pd substrate atoms are expelled from the surface, usually forming Pd defects which increase the LEIS signal from palladium at angles close to grazing incidence.[20,24] However, such an increase was not observed in the present case. Hence, we conclude that intermixing/alloying does not occur during deposition at 150 K.

3.2. Thermal Stability. To investigate the stability of deposited films upon increasing temperatures, temperature-programmed desorption (TPD) experiments were performed. However, desorption of Ga was not observed in the experimentally accessible temperature range up to 1200 K.

The surface compositions as obtained from temperature-programmed LEIS measurements are displayed in Figure 3 for films of various initial gallium coverages (solid and dashed black lines, respectively). Generally, all curves show a decreasing Ga surface fraction with increasing sample temperature. As desorption of Ga does not take place, the observed changes in surface composition can be unequivocally assigned to alloying processes and diffusion of Ga surface atoms into

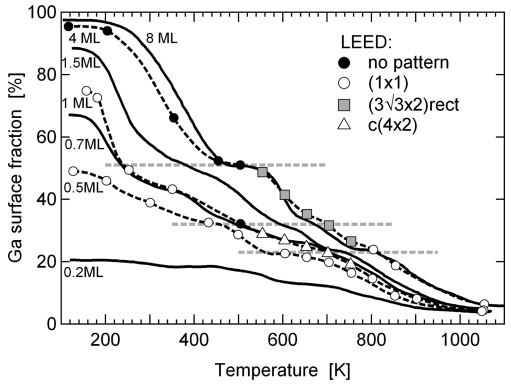

Figure 3. Top-layer Ga content (obtained by LEIS) as a function of temperature for various initial gallium coverages on Pd(111). A constant heating rate of 1 K/s was applied. Data are shown as smoothed curves; for a set of raw data see the Supporting Information, Figure S2. Dashed horizontal lines indicate surface fractions that appear to be more stable. The observed LEED patterns are indicated by symbols.

deeper Pd layers. As is immediately evident, the alloying processes take place in several steps. Most pronounced is the onset of alloying, starting at around 200 K for low coverages and shifting to higher temperatures for thicker films. Partially we attribute this shift to a kinetic effect as it takes longer times (equivalent to higher temperatures) for the Pd substrate atoms to reach the surface of thicker films. To prove this idea, the experiment was repeated with the heating rate reduced by a factor of 10. As expected, the onset temperatures shifted slightly (by about 20−40 K) toward lower temperatures. Furthermore we note that with increasing thickness the films become more closed (compare Figure 2), thus providing an enhanced resistivity for up-diffusion of Pd as the migration channel changes from surface toward bulk diffusion.

The initial first concentration decrease comes to a halt, especially for the 4 and 8 ML exposures, at a Ga surface content of ∼50%, indicating that this composition has an enhanced stability. At higher temperatures two other, less pronounced plateaus are visible at Ga surface fractions of ∼0.33 and ∼0.25 (see dashed lines in Figure 3). Finally, above 800 K all curves decline steadily, indicating diffusion of Ga atoms into the bulk of the Pd sample. Even at the highest temperatures the Ga content does not fall below ∼5% due to the tendency of Ga for surface segregation (i.e., to have a surface concentration exceeding that in the underlying bulk crystal) as already mentioned in the Experimental Section.

The 0.2 ML preparation does not show a change in surface composition up to ∼500 K. Nevertheless, already at temperatures of ∼250 K alloying takes place between the Ga adlayer and the Pd surface. As the Ga surface fraction measured by LEIS remains unaltered, alloying obviously is essentially restricted to the Pd surface layer (i.e., without Ga atoms moving into subsurface layers). That alloying takes place at 250 K is evident from the signal at grazing incidence in polar ICISS scans (not shown): After annealing to 250 K the backscattering signal from Pd atoms increases markedly in this angular range, indicating the creation of Pd step- and adatoms being pushed out of the surface due to their replacement by Ga. Upon further annealing the ICISS intensity stays high until 550 K, where the step/adatom signal decreases due to a smoothing of the alloyed surface.

3.3. Structure. *LEED.* Electron-diffraction experiments were performed at submonolayer (0.5 ML), monolayer (1 ML), and multilayer (4 ML) coverages of gallium. The observed LEED patterns are indicated by the symbols overlaid in Figure 3 on the respective LEIS curves with the same initial Ga coverage.

The submonolayer measurements (0.5 ML) revealed a (1 × 1) pattern at all temperatures. Upon annealing to temperatures beyond 200 K, the quality of the (1 × 1) LEED pattern deteriorated considerably, indicating structural rearrangements of the surface due to the onset of alloying. At temperatures above 650 K, the intensities of (1 × 1) spots start to increase again due to the loss of Ga into Pd bulk and the gradual reappearance of the clean Pd(111) surface.

Similarly, at a coverage of 1 ML a (1 × 1) pattern was visible after deposition at 150 K, but worsened after annealing. At a temperature of 500 K the LEED spots became essentially invisible, indicating almost complete loss of long-range order. At and above 550 K the spots of a weak (2 × 2) pattern reappeared. However, at low electron energies (∼50 eV) a few additional faint and diffuse spots were visible, suggesting that actually a c(4 × 2) structure was present (which contains the (2 × 2) spots as a subset). However, due to the extreme

dx.doi.org/10.1021/jp407337q | J. Phys. Chem. C 2013, 117, 19558−19567

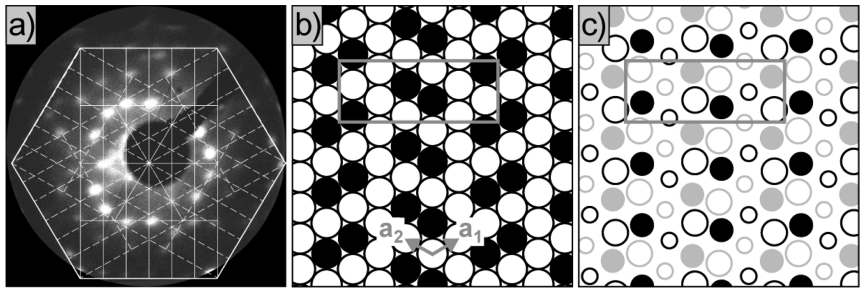

Figure 4. (a) LEED image (E = 60 eV) of the three-domain $(3\sqrt{3} \times 2)$rect structure after deposition of approximately 4 ML gallium at 600 K, superimposed with the reciprocal lattices of the three domains. The outer hexagon connects the (1 × 1) diffraction spots of the Pd(111) substrate. (b) Idealized model of the fcc $(\bar{1}11)$ equivalent lattice plane of Pd_2Ga with all atoms residing on fcc lattice positions. Open (filled) symbols denote Pd (Ga) atoms. (c) Realistic model of the fcc $(\bar{1}11)$ equivalent plane of Pd_2Ga. Circles which are smaller than those in panel b denote out-of-plane atoms. Black (gray) atoms are above (below) the drawing plane. The $(3\sqrt{3} \times 2)$rect unit cell is marked by rectangles.

weakness of these spots, this assignment is not unambiguous. Above 800 K only a (1 × 1) pattern remained.

The multilayer 4 ML film exhibited no LEED pattern at all in the as-deposited state as well for temperatures up to 500 K. At higher temperatures, spots of a 3-domain $(3\sqrt{3} \times 2)$rect structure developed, until above 800 K again a (1 × 1) structure, indicative of the reemerging Pd(111) surface, became visible. The quality of the $(3\sqrt{3} \times 2)$rect structure could be improved, if deposition of the multilayer film was carried out at an elevated sample temperature of 600 K. The corresponding LEED image is shown in Figure 4a together with the expected reciprocal lattice. As this pattern is observed for multilayer amounts of Ga and at elevated temperature, it is tempting to relate it to the formation of a bulk-like Pd−Ga intermetallic film. From the many existing Pd_xGa_y intermetallic compounds, formation of Pd_2Ga seems to be most likely for various reasons: (i) Pd_2Ga is the thermally most stable intermetallic phase. (ii) It contains 33% of Ga, which is compatible with the Ga surface fraction ranging from 20 to 50% as measured by LEIS (Figure 3). (iii) The crystal structure of Pd_2Ga is of the orthorhombic Co_2Si type of space-group symmetry *Pnma*. For this structure type a symmetry relation exists to the fcc structure of the underlying face-centered cubic (fcc) Palladium substrate, meaning that the atomic sites of Pd_2Ga can be viewed as a distorted fcc structure[25] (for a graphical representation of the idealized, nondistorted bulk Pd_2Ga unit cell see the Supporting Information, Figure S1). (iv) Even more, the lattice constants of the orthorhombic Pd_2Ga unit cell fit nicely to intermetallic distances of the Pd substrate with misfits below 6% for each axis of the orthorhombic unit cell (see Table 1). (v) The ***a***-axis of Pd_2Ga has a particular small misfit of only 0.5%, implying that row-matching can be relatively easily achieved, if ***a*** aligns along one of the close-packed ⟨101⟩ directions of the Pd substrate. All together, epitaxial growth of Pd_2Ga films with a fcc{111}-equivalent surface normal and the *a* axis aligned parallel to one of the close-packed directions of the Pd(111) surface appears to be highly probable.

Table 1. Relation between the Pd_2Ga Unit Cell and the Associated Vectors of the Face-Centered Cubic Lattice of the Palladium Substrate[a]

Pd_2Ga unit cell		associated lattice vectors of Pd		
basis vector	length [pm]	length [pm]	direction	misfit
a	547.6	550.3	[101]	+0.5%
b	405.7	389.1	[010]	−4.1%
c	779.4	825.4	$[^3/_2\ 0\ ^3/_2]$	+5.9%

[a]Structural parameters for Pd_2Ga are taken from ref 25. and are in agreement with more recent data of ref 26. The latter work also provides a 3D visualization of the Pd_2Ga bulk structure.

In Figure 4b a model of an idealized Pd_2Ga phase with an fcc $(\bar{1}11)$-equivalent surface (corresponding to the $Pd_2Ga(013)$ plane) is shown. In this idealized model, all atoms of Pd_2Ga are located on perfect fcc lattice sites. As can be seen, the resulting unit cell has rectangular symmetry with 12 atoms per unit cell and Pd:Ga = 2:1 stoichiometry. In Park−Madden matrix notation this overstructure is termed $\begin{pmatrix} 3 & -3 \\ 2 & 2 \end{pmatrix}$ with respect to the unit vectors $\mathbf{a}_1$ and $\mathbf{a}_2$ of the underlying Pd(111) substrate as indicated in Figure 4b. In the extended Wood-notation it is denoted as $(3\sqrt{3} \times 2)$rect. Hence it exhibits exactly the experimentally observed periodicity. For the corresponding surface of the real (i.e., nonidealized) truncated Pd_2Ga bulk structure, the atomic positions within the unit cell are somewhat altered: The perfect hexagonal atomic arrangement is destroyed and some buckling is introduced. However, the overall periodicity and the stoichiometry of the surface are maintained, see Figure 4c. Hence the formation of a Pd_2Ga-like film provides a reasonable and straightforward explanation of the observed diffraction pattern. It is particularly noteworthy that for Pd_2Ga two inequivalent types of fcc{111}-derived lattice planes exist. Whereas the $(\bar{1}11)_{fcc}$ and $(\bar{1}\,\bar{1}1)_{fcc}$ planes exhibit a $(3\sqrt{3} \times 2)$rect unit cell as shown above, the $(111)_{fcc}$ and $(1\bar{1}1)_{fcc}$ planes form $\begin{pmatrix} 3 & 3 \\ -2 & 2 \end{pmatrix}$ or $(2\sqrt{3} \times 3)$rect unit cells, which are incompatible with the experimental observation. It is a particular hallmark of these latter lattice planes, that they do not contain the *a* axis of Pd_2Ga, i.e., the axis which has an almost perfect row matching with the close-packed ⟨101⟩ directions of palladium. Accordingly, epitaxial growth of this type of surfaces is less likely and only the $(3\sqrt{3} \times 2)$rect structure is observed.

Finally, we comment on the diffuse c(4 × 2) pattern observed after annealing of 1 ML Ga to temperatures between 550 and 750 K. According to our LEIS measurement at these temperatures the Ga surface fraction is around 25%, which fits to a c(4 × 2) structure with one Ga atom per unit cell. A model for this structure is depicted in Figure 10a. It is similar to a (2 × 2) overlayer, with every second "vertical" Pd−Ga row shifted by one atom along the row. Note also the close relationship of this structure to that of the $(3\sqrt{3} \times 2)$rect phase (Figure 4c). Both structures contain similar subunits, i.e., "vertical" rows of either pure Pd or of alternating Pd and Ga

dx.doi.org/10.1021/jp407337q | J. Phys. Chem. C 2013, 117, 19558−19567

atoms. This close relationship can also be brought out in the notation as the c(4 × 2) structure can also be termed $(\sqrt{3} \times 2)$rect or $\begin{pmatrix} 1 & -1 \\ 2 & 2 \end{pmatrix}$ in matrix notation.

ICISS. Azimuthal ICISS scans of clean Pd(111) as well as of as-deposited and annealed Ga films are depicted in Figure 5.

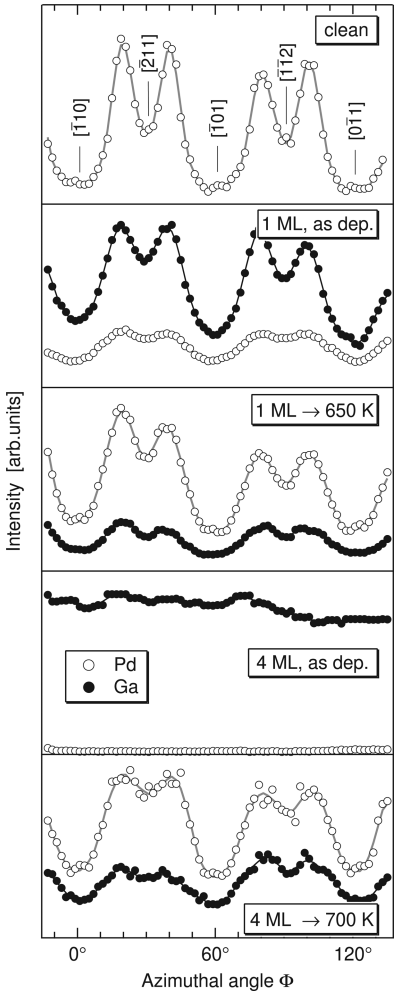

Figure 5. Azimuthal ICISS scans for clean and various Ga-covered Pd(111) surfaces. Scans were taken at $\psi = 11°$. Filled (open) symbols denote the Ga (Pd) signal.

The clean surface exhibits a 6-fold pattern with pronounced minima along the nearest neighbor <1̄10> and next-nearest neighbor <2̄11> directions, characteristic for the hexagonal Pd(111) surface structure. For the monolayer film the same type of pattern is observed, no matter whether the Ga or the Pd-related signal is monitored. The minima are less pronounced, indicating a less ordered surface. After annealing to 650 K, i.e., to a temperature where LEED has shown the faint c(4 × 2) pattern, the azimuthal scans are essentially the same as before, only the intensity ratio between Ga and Pd is roughly inverted due to the progressive alloying of the Ga film, which decreases the Ga fraction in the surface layer. The similarity of the observed azimuthal scans with that measured for clean Pd(111) indicates, that in the bimetallic c(4 × 2)-like film the local lateral atomic arrangement is quite similar to that of the clean fcc(111) surface and that the periodicity observed by LEED is due to the chemical difference of the surface atoms (Pd, Ga) rather than due to strong structural rearrangements of the surface layer.

After deposition of multilayer films (4 ML), the 6-fold periodicity of the ICISS signal can no longer be discerned. In agreement with the nonobservable LEED pattern this indicates the complete loss of structural order of the as-grown surface. After annealing to 700 K (where LEED shows the $(3\sqrt{3} \times 2)$rect pattern) the 6-fold periodicity reappears. This observation is compatible with a distorted quasi-hexagonal structure, similar to that of the $(3\sqrt{3} \times 2)$rect plane as depicted in Figure 4c.

The structure of the bimetallic films was investigated further by polar ICISS scans, where the angle of incidence (measured relative to the surface) was varied, while the azimuthal orientation was kept fixed. As an example Figure 6 shows

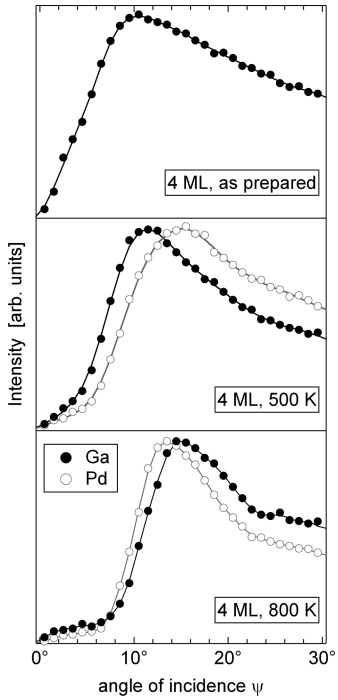

Figure 6. Polar ICISS scans for 4 ML Ga films on Pd(111) after annealing to different temperatures. Filled (open) symbols denote the Ga (Pd) signal. Note the inversion of the onsets of the Ga and Pd signal, respectively, after annealing to 800 K. All spectra are normalized to the same maximum height to allow for a better comparison of critical angles. Azimuthal direction was [2̄11].

polar ICISS scans of 4 ML of Ga, taken after deposition as well as after annealing to 500 and 700 K, respectively. Characteristic for the as-deposited film is an almost straight increase of the backscattering intensity, starting directly at grazing incidence (Figure 6, top). This is indicative of a disordered and rough film, and is in agreement with the previous conclusions based on the uptake curve (Figure 2), LEED and azimuthal ICISS scans, from which nonperfect layer-by layer growth of a quasi-amorphous film has been deduced. After annealing to 500 K (i.e., to the metastable plateau region visible in Figure 3), more well-behaved signals are observed (Figure 6, center): The intensity increase starting immediately at grazing incidence is reduced (although not completely) and clear focusing peaks are observed for both Ga and Pd, indicating the presence of an ordered surface. Notably, the critical angles (i.e., the angle where the intensity has risen to 50% of its maximum value)

dx.doi.org/10.1021/jp407337q | J. Phys. Chem. C 2013, 117, 19558−19567

associated with the focusing peaks of the Ga and the Pd signal are shifted with respect to each other, with the Ga signal rising 2° earlier than the Pd signal. As explained in more detail in ref 17 for the analogous Zn/Pd(111) system, such large differences arise primarily from a buckled surface with Pd and Ga atoms located at different heights. As the Ga signal rises already at lower angles than the Pd signal, this implies that the Ga atoms are located somewhat higher than the Pd surface atoms.

After annealing to 800 K, the difference in critical angles is markedly reduced and even inverted (see Figure 6, bottom). Now the Pd signal rather than the Ga signal rises first, indicating a smaller and even inverted buckling with Pd atoms located above their Ga counterparts

In Figure 7 the evolution of the difference $\Delta\Psi_C = \Psi_{C,Pd} - \Psi_{C,Ga}$ between the critical angles of Pd and Ga is shown as a

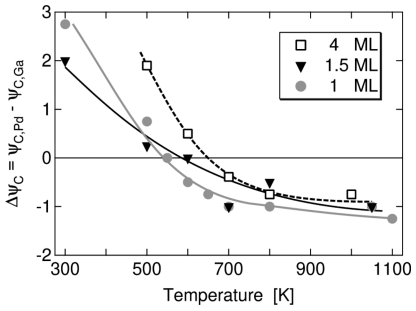

Figure 7. Difference $\Delta\psi_C$ in critical angles for backscattering from Pd and Ga atoms as a function of annealing temperature for Ga films of various thicknesses on Pd(111). $\Delta\psi_C$ serves as a measure for surface buckling. Positive values indicate that Ga atoms are located above their Pd counterparts; negative values indicate the opposite behavior.

function of temperature for films with initial Ga coverages of 1, 1.5, and 4 ML. In all cases a qualitatively similar behavior is observed. At low temperatures $\Delta\Psi_C$ is positive, indicating a Ga-up/Pd-down buckling, whereas at higher temperatures the inverted behavior is found. With increasing initial coverage the zero-crossing of the three curves shifts to higher temperatures. When the crossing temperatures are converted to Ga surface coverages with the help of Figure 3, it turns out that the inversion takes place in a narrow coverage window with Ga surface fractions between 29 and 35%. This suggests that the buckling behavior is governed by the Ga content of the bimetallic surface.

The present findings seem to be at variance with our previous publication, stating that buckling is not observed for PdGa films on Pd(111).[11] However, these early results were taken only in a limited coverage/temperature range (~1.5 ML, 500 K) where buckling is close to zero.

A closer inspection of Figure 6 reveals further differences. In the case of the 500 K annealed film, both critical angles are shifted to smaller angles and the intensity increase is less sharp than after annealing to 800 K. Qualitatively similar effects are generally observed, if spectra are measured at elevated temperatures due to the enhanced (dynamic) disorder caused by the thermal motion of the atoms.[20] In analogy to that, we attribute the shift and broadening in the present measurements to an enhanced static disorder of the (primarily vertical) atomic positions of the 500 K annealed film. (As the scattering process is fast compared to the thermal motion of the atoms, ion-scattering does not discriminate between dynamic and static disorder.) A better ordering of the 800 K annealed film with less surface defects is also evident from the lower intensities observed in the shadowing region close to grazing incidence.

4. Ga/Pd(110)

4.1. Growth. Figure 8 depicts the normalized top-layer Ga signal as a function of the deposition time for evaporation onto

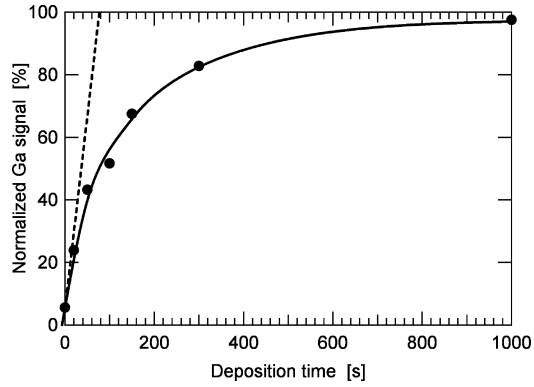

Figure 8. Normalized gallium content versus deposition time on Pd(110) as obtained from low-energy ion scattering. The deposition temperature was 150 K. The solid line is a guide to the eye.

the Pd(110) surface kept at 150 K. Qualitatively, the observed nonlinear increase is similar to that measured for Ga/Pd(111), compare Figure 2. However, in the present case the deviation from a linear signal increase is stronger, indicating a more three-dimensional growth behavior. In addition, near grazing incidence measurements of small Ga coverages (0.3 ML, not shown) exhibit a pronounced increase of the Pd signal, indicating intermixing of Ga and Pd already at 150 K. The deposition rate (in ML/s) was calculated from the value measured for Ga/Pd(111), taking into account the lower atom density of the (110) surface as compared to (111). This results in a deposition rate of 1 ML/80 s. The corresponding growth curve expected with this deposition rate in the case of perfect layer-by-layer growth is shown by the dashed line in Figure 8. As can be seen, data points deviate significantly from this line, due to a strongly developed three-dimensional growth mode and intermixing at small coverages.

4.2. Thermal Stability. As for Ga/Pd(111), thermal desorption of gallium was not observed in the temperature range up to 1200 K. The results of temperature-programmed LEIS measurements (Figure 9) parallel that of Ga/Pd(111) in many respects:

(i) Temperature-induced alloying sets in around 200 K, with the onset temperature shifting toward higher temperatures for thicker films curves.
(ii) The initial alloying-induced drop in the Ga signal comes to a first halt at a Ga fraction of ~50% (4, 6, and 12 ML curves).
(iii) A second plateau-like region behavior is observed for Ga fractions around 30%.
(iv) Above ~800 K all curves decline steadily due to diffusion of Ga into the Pd bulk.
(v) Even at the highest temperatures the measured Ga content remains above ~5%, i.e., above the Ga concentration in the bulk (segregation tendency).

Surprisingly, in some of the measured curves (in particular for 12 ML) the normalized Ga signal does not only show plateau-like regions but even an intermediate increase with

dx.doi.org/10.1021/jp407337q | J. Phys. Chem. C 2013, 117, 19558−19567

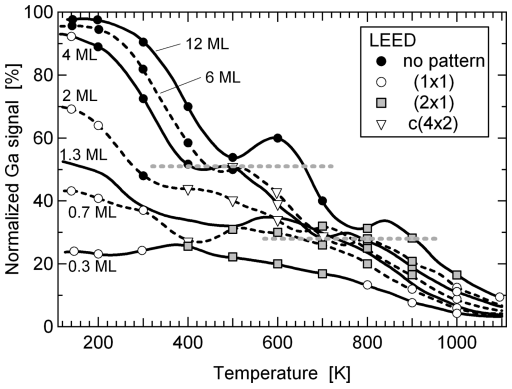

Figure 9. Normalized Ga content (obtained by LEIS) as a function of temperature for various initial gallium coverages on Pd(110). A constant heating rate of 1 K/s was applied. Dashed horizontal lines indicate surface fractions that appear to be more stable. The LEED patterns observed after annealing to the indicated temperatures are indicated by symbols drawn onto the LEIS curves with the same initial Ga coverage.

rising temperature. In our opinion, this does not indicate a true increase of the Ga surface content. Rather we suppose that either neutralization effects change or that our assumption that in the chosen measurement geometry only top-layer atoms contribute to the LEIS signal is no longer strictly valid. In both cases we have to conclude that the normalized Ga signal shown in Figure 9 maybe somewhat off the true Ga surface fraction.

4.3. Structure. *LEED.* The results of our LEED investigations are indicated by the symbols overlaid onto the LEIS curves in Figure 9. At small coverages and low temperatures only the (1×1) pattern of the Pd(110) substrate is observed. At coverages exceeding 4 ML diffraction spots could no longer be observed for the as-deposited films as well as for films annealed to intermediate temperatures ($\lesssim$500 K), indicating a surface and near-surface region without long-range order. After annealing to "high" temperatures, i.e. to temperatures sufficient for obtaining a Ga fraction of ~30% (as measured by LEIS), i.e., $\gtrsim$500 K for 0.7 ML, $\gtrsim$800 K for 12 ML, a (2×1) pattern appeared. We attribute this pattern to the formation of Pd−Ga rows along the close-packed $[\bar{1}10]$ direction as shown schematically in Figure 10b. The ideal Ga surface fraction of this structure is 50%, which is in contrast to the measured values of $\lesssim$30%. Two possible explanations of this apparent contradiction are at hand. First, as discussed above, the measured LEIS signal may not accurately represent the true surface composition. However, the error introduced here is probably not large enough to account for the rather large difference of 20%. A second explanation of the measured low Ga content is the existence of (2×1) patches with a local 1:1 surface composition, together with regions of lower or even vanishing Ga content. Support for this latter scenario comes from the fact, that the (2×1) pattern is observed even for initial coverages of 0.3 ML, where a full (2×1) structure with a 1:1 Ga-to-Pd ratio obviously is not possible.

The (2×1) pattern is observed over a large range of initial Ga coverages (0.3−12 ML). At least for the higher coverages is tempting to speculate about the formation of Pd_2Ga-like surface-near films in analogy to the ideas presented for deposition onto the Pd(111) surface. Due to the orthorhombic structure of Pd_2Ga six nonequivalent fcc(110)-like lattice planes exist for Pd_2Ga. Of these six types of planes the $(\bar{1}01)$-like plane (corresponding to the $Pd_2Ga(001)$ plane) is particularly prone for epitaxial growth on Pd(110), as it is the only one that contains the ***a***-axis of Pd_2Ga (which, as shown in Table 1, has only a 0.5% misfit with the close-packed $[\bar{1}10]$ direction of palladium) as an in-plane direction. Furthermore, for this lattice plane the ***c***-axis (which has the largest misfit with the Pd substrate) points normal to the surface, where stress release is easily possible. As it turns out, this surface orientation is also the only one that exhibits a (2×1) in-plane periodicity (where the (2×1) notation is relative to the atomic sites of an ideal fcc $(\bar{1}01)$ plane). Along the **c**-axis, the repeating cell of the Pd_2Ga crystal can be viewed as a stack of six fcc $(\bar{1}01)$ like planes (see the Supporting Information, Figure S1). Four of these consist of close-packed buckled Pd−Ga rows (two planes with Pd-up/Ga-down and two planes with Ga-up/Pd-down buckling), two planes contain only Pd atoms, arranged in (2×1) buckled rows. Buckling amplitudes are 40 − 66 pm (peak-to-peak). Hence formation of Pd_2Ga films is a natural explanation for the observed (2×1) periodicity of annealed multilayer Ga films. The (2×1) structures observed at low initial Ga coverages can then be considered as the initial phases of Pd_2Ga growth. However, for multilayer Pd_2Ga films, it is unclear, which of the six stacked fcc $(\bar{1}01)$-like planes actually forms the terminating layer or whether several terminations coexist. If all possible terminations occurred in equal fractions, surface regions with local 1:1 stoichiometry would coexist with pure Pd terminating layers, resulting in a global Ga surface content of 33%, in agreement with the LEIS fractions measured for the (2×1) structures. However, it should be clearly pointed out at this stage, that, as for Ga/Pd(111), too, formation of bulk-like a Pd_2Ga film, although giving a reasonable and straightforward explanation of the experimental observations, cannot be unequivocally deduced from our data as only surface compositions are measured by LEIS.

At intermediate coverages (2−4 ML) and intermediate annealing temperatures a streaky $c(4 \times 2)$ diffraction pattern is

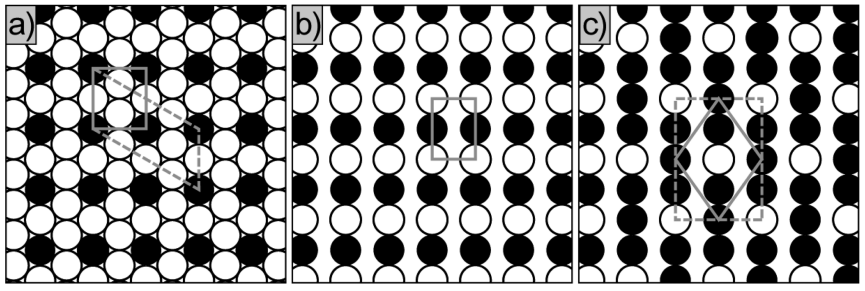

Figure 10. Top-layer structural models for (a) $c(4 \times 2)$ Ga/Pd(111), (b) (2×1) Ga/Pd(110), and (c) $c(4 \times 2)$ Ga/Pd(110). Filled (open) circles denote Ga (Pd) atoms. The primitive (centered) unit cells are depicted by the solid (dashed) gray lines.

dx.doi.org/10.1021/jp407337q | J. Phys. Chem. C 2013, 117, 19558−19567

observed with measured Ga fractions slightly below 50%. In principle a c(4 × 2) pattern would be consistent with a Ga surface content of 50%. However, from the considerations presented above, we expect that for (local) Ga fractions of 50% a (2 × 1) structure is formed. As the c(4 × 2) structure is observed at lower annealing temperatures (and hence higher Ga surface fractions) we propose that the c(4 × 2) structure originates from patches with a local Ga content of 75% as schematically shown in Figure 10c. Such a structure appears to be plausible for two reasons: The minority Pd atoms are quite evenly distributed, so Ga−Pd bonds (which are stronger than both Ga−Ga as well as Pd−Pd bonds[29]) are optimized. Furthermore, this structure is a natural predecessor for the (2 × 1) structure appearing at higher temperatures, as it can be transformed into the (2 × 1) phase just by replacing more Ga atoms by Palladium.

ICISS. Polar ICISS scans of a 4 ML Ga film are shown in Figure 11. The as-deposited film (Figure 11a) shows an immediate, almost linear rise of the Ga signal starting right at the grazing incidence. This indicates a rough and disordered surface, in agreement with our earlier conclusions. Mild annealing does not improve the situation. Even at 700 K, i.e., just before evolution of the (2 × 1) phase, the surface still appears to be rough, exhibiting both Ga and Pd defects (the latter as a consequence of the thermally induced alloying process), see Figure 11b. Only after formation of the (2 × 1) structure is the quality of the alloyed film markedly improved as indicated by the reduced intensity close to grazing incidence and the presence of clear focusing peaks (Figure 11c). The Pd signal rises well before that of Ga, indicating a significant surface buckling with Pd atoms residing higher than Ga atoms.

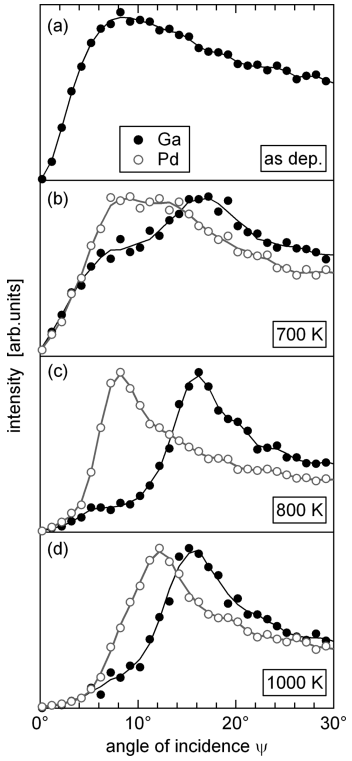

Figure 11. Polar ICISS scans for 4 ML Ga films on Pd(110) after annealing to different temperatures. Filled (open) symbols denote the Ga (Pd) signal. All spectra are normalized to the same maximum height to allow for a better comparison of critical angles.

After annealing to 1000 K the Pd focusing peak has shifted upward toward its clean surface value, showing that the buckling is reduced at higher temperatures (Figure 11d). Essentially the same qualitative behavior was observed for films with initial coverages between 0.7 and 12 ML. In all cases relatively defect-free films with maximum Pd-up/Ga-down buckling (as inferred from the difference in critical angles for the Pd and Ga signal, respectively) form at the temperature necessary for obtaining the (2 × 1) phase.

Azimuthal ICISS scans are shown in Figure 12. Analogous to the measurements presented for Ga/Pd(111) and in agreement

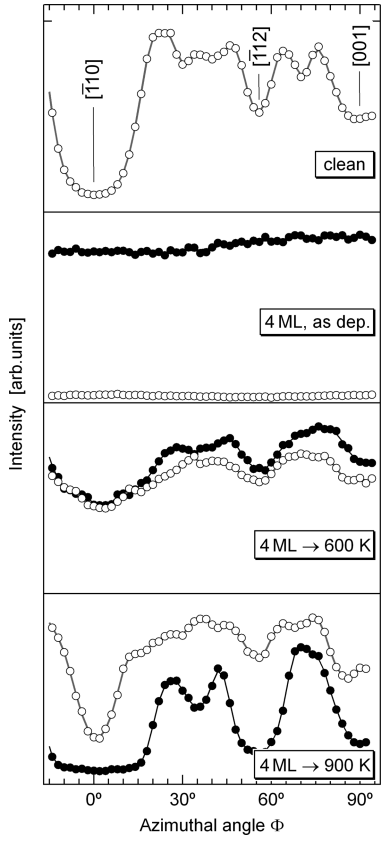

Figure 12. Azimuthal ICISS scans for clean and 4 ML Ga/Pd(110) annealed to various temperatures. Scans were taken at $\psi = 10°$. Filled (open) symbols denote the Ga (Pd) signal.

with our LEED results (no diffraction pattern at high coverages and "low" temperatures) a structureless azimuthal spectrum is obtained after deposition of 4 ML. After annealing to 600 K (i.e., in the c(4 × 2) region) the spectra gain some structure with minima along the same directions as for clean Pd(110), indicating that nearest, second-, and third-nearest neighbor directions are preserved. After annealing to 900 K (i.e., formation of the (2 × 1) structure) the azimuthal scan shows pronounced structures, indicative of a well ordered surface. Again the three most pronounced minima coincide with that of the clean surface. Nevertheless the azimuthal spectra are not perfect replicas of the clean surface scan. This is a consequence of the rather large buckling present on the (2 × 1) surface, which also alters the azimuthal scans as these are measured at small angles of incidence ($\psi = 10°$, i.e., close to grazing incidence). In particular, for the low-lying atoms (Ga) the depth/width of the minima should increase, whereas for the high-lying atoms (Pd) the depth/width is expected to decrease

dx.doi.org/10.1021/jp407337q | J. Phys. Chem. C 2013, 117, 19558−19567

(relative to the clean surface spectrum), in agreement with the experimental observation.

5. DISCUSSION AND CONCLUSIONS

In this final section we compare the present results for Ga/Pd(111) and Ga/Pd(110) with those of the related systems Zn/Pd(111) and Zn/Pd(110) as obtained by LEIS as well as other methods.[14,15,17−19]

With respect to the growth mode at 150 K (exception: 300 K for Zn/Pd(110)) the four systems behave similarly. In all cases the growth curves obtained by LEIS indicate a nonperfect layer-by layer growth, i.e., several layers of the deposited material are simultaneously exposed. In part this may be due to the low deposition temperature, reducing the adatom mobility across steps of the growing structures.

With respect to formation of an intermixed interface during deposition Zn and Ga behave similarly: On the close-packed Pd(111) such an intermixing does not occur at 150 K, whereas on the more open Pd(110) surface an intermixed interface is formed. This appears reasonable, as on the open fcc(110) surfaces a small kinetic barrier for exchange processes can be more easily achieved by a concerted motion of atoms.[27]

In contrast, zinc and gallium behave quite differently with respect to thermal desorption. While Zn can be desorbed completely,[15,16] no desorption was observed for gallium in the experimentally accessible temperature range up to 1200 K. This is a consequence of the much higher cohesive energy of gallium and Pd−Ga intermetallics as compared to that of zinc and Pd−Zn: The cohesive energy of Zn is −1.1 eV/atom,[28] and that of Ga is more than double as high (−2.8 eV/atom).[29] Analogously, the cohesive energy for PdGa (−3.9 eV/atom) exceeds that of PdZn (−3.0 eV/atom).[28,29] A further difference between Zn and Ga concerns the structure of the as-deposited films. Zinc forms epitaxial films, which at higher coverages adopt a Zn(001)-like structure independent of substrate orientation.[19] In contrast, gallium tends to form disordered/amorphous films, possibly a remainder of the low melting point of gallium (303 K).

Also the onset temperature for thermally induced alloy formation differs between both materials: For Ga this process sets in around 200 K on both Pd(111) and Pd(110), whereas for Zn temperatures of 300 (on Pd(111)) and 500 K (on Pd(110)) are necessary.[19] This difference can be understood as a consequence of the larger thermodynamic driving force for Pd−Ga compound formation as compared to Pd−Zn. The orientation-independent onset temperature for Ga is attributed to the fact that on both Pd(111) and Pd(110) amorphous Ga and Pd−Ga films are formed.

Common to all systems is the formation of metastable surface configurations with a global 1:1 composition as indicated by the presence of clear plateaus in the surface composition when the temperature is raised. For Zn films on Pd(111) and Pd(110) this is the only metastable surface composition, while for Ga films further, although less pronounced, stability plateaus were observed. This parallels the behavior of the bimetallic bulk phase diagrams, which for Pd−Ga is considerably more complex, exhibiting a large number of different intermetallic phases. Furthermore, for Zn/Pd the 1:1 plateau goes in hand with the formation of an ordered (2 × 1) surface structure, whereas for Ga/Pd the surface is disordered at this stage. Ordered surface structures of Ga/Pd are observed by LEED and ICISS only in the regions of the other, weakly developed stability plateaus.

The (2 × 1) structures observed for Zn/Pd(111), Zn/Pd(110), and also Ga/Pd(110) at higher temperatures are attributed to the formation of densely packed rows of atoms containing Pd and Zn (or Ga) atoms in alternating order. This structural motive is also present in the $(3\sqrt{3} \times 2)$rect and c(4 × 2) models presented for Ga/Pd(111) and is a consequence of the strong Pd−M bonding as compared to Pd−Pd and M−M (M═Zn,Ga).

When several monolayers of the film material are deposited at temperatures around 500−600 K for both Zn[15] and Ga on Pd(111) the same $(3\sqrt{3} \times 2)$rect LEED pattern is observed. As shown in the present work for Ga/Pd(111), this pattern is most probably caused by the formation of a bulk-like Pd_2Ga near-surface intermetallic phase. For Zn/Pd(111) this pattern was also attributed to the formation of a bulk-like intermetallic film, however, with 1:1 stoichiometry.[15,30] Hence for both M═Zn and M═Ga the observed $(3\sqrt{3} \times 2)$rect pattern indicates the presence of bulk-like Pd-M intermetallic phases, which however are related to structurally and stoichiometrically distinctly different intermetallic phases (PdZn and Pd_2Ga, respectively).

The atomic buckling of the films as revealed by polar ICISS scans depends on the surface orientation. On Pd(110) always a Pd-up/M-down buckling is observed, for both M═Zn and M═Ga. For Ga/Pd(110) this buckling is particularly large. On Pd(111) a more complex behavior is observed, as the buckling changes sign when the sample is annealed. At low temperatures a M-up/Pd-down configuration exists, which inverts to a (weak) Pd-up/M-down buckling for both materials roughly around 600 K. Both from theory as well as from experiment this change in buckling behavior for Zn/Pd(111) has been associated with the transition from a multilayer near-surface intermetallic PdZn film to a monolayer-like situation. We cannot exclude this explanation also for Ga/Pd(111); however, it would be inconsistent with our hypothesis that at these enhanced temperatures a bulk-like Pd_2Ga film is formed. Rather, we suggest that the inversion of buckling is related to the formation of a Pd_2Ga-like surface configuration.

With respect to the catalytic behavior of near-surface PdZn films in methanol steam reforming, a high CO_2 selectivity was only reported for multilayer PdZn films, exhibiting a Zn-up/Pd-down buckling on Pd(111).[13] For Ga/Pd(111) qualitatively the same buckling behavior is observed, nevertheless oxidized Ga species are not formed under MSR conditions and CO_2 is only marginally produced in experiments on polycrystalline Pd foils.[6,11] Obviously, but perhaps not too surprisingly, surface buckling of the bimetallic film is not a sufficient criterion for the ability to form a bimetal/oxide interface under reaction conditions and to achieve high catalytic CO_2 selectivity.

■ ASSOCIATED CONTENT

Ⓢ Supporting Information

Figure S1: Relation between Pd_2Ga unit cell and fcc lattice. Figure S2: Comparison of raw and smoothed temperature-programmed LEIS data of Ga/Pd(111). This material is available free of charge via the Internet at http://pubs.acs.org.

■ AUTHOR INFORMATION

Corresponding Author

*E-mail: norbert.memmel@uibk.ac.at.

Notes

The authors declare no competing financial interest.

■ ACKNOWLEDGMENTS

Financial support by the Austrian Science Fund (Grant P20892-N19) and by a PhD-grant (W.S.) of the University of Innsbruck is gratefully acknowledged. We thank Reinhold Pramsoler for the excellent technical assistance.

■ REFERENCES

(1) Palo, D. R.; Dagle, R. A.; Holladay, J. D. Methanol Steam Reforming for Hydrogen Production. *Chem. Rev.* **2007**, *107*, 3992−4021.

(2) Iwasa, N.; Mayanagi, T.; Ogawa, N.; Sakara, K.; Takezawa, N. New Catalytic Functions of Pd-Zn, Pd-Ga, Pd-In, Pt-Zn, Pt-Ga and Pt-In Alloys in the Conversion of Methanol. *Catal. Lett.* **1998**, *54*, 119−123.

(3) Iwasa, N.; Takezawa, N. New supported Pd and Pt Alloy Catalysts for Steam Reforming and Dehydrogenation of Methanol. *Top. Catal.* **2003**, *22*, 215−224.

(4) Penner, S.; Lorenz, H.; Jochum, W.; Stöger-Pollach, M.; Wang, D.; Rameshan, C.; Klötzer, B. Pd/Ga_2O_3 Methanol Steam Reforming Catalysts: Part I. Morphology, Composition and Structural Aspects. *Appl. Catal., A* **2009**, *358*, 193−202.

(5) Lorenz, H.; Penner, S.; Jochum, W.; Rameshan, C.; Klötzer, B. Pd/Ga2O3Methanol Steam Reforming Catalysts: Part II. Catalytic Selectivity. *Appl. Catal., A* **2009**, *358*, 203−210.

(6) Lorenz, H.; Rameshan, C.; Bielz, T.; Memmel, N.; Stadlmayr, W.; Mayr, L.; Zhao, Q.; Soisuwan, S.; Klötzer, B.; Penner, S. From Oxide-Supported Palladium to Intermetallic Palladium Phases: Consequences for Methanol Steam Reforming. *ChemCatChem* **2013**, *5*, 1273−1285.

(7) Sa, S.; Silva, H.; Brandao, L.; Sousa, J. M. Catalysts for Methanol Steam Reforming—A Review. *Appl. Catal., B* **2012**, *99*, 43−57.

(8) Behrens, M.; Armbrüster, M. Methanol Steam Reforming. In *Catalysis for Alternative Energy Generation*; Springer: New York, 2012; pp 175−235.

(9) Föttinger, K. PdZn Based Catalysts: Connecting Electronic and Geometric Structure with Catalytic Performance. *Catalysis* **2013**, *25*, 77−117.

(10) Leary, R.; de la Pena, F.; Barnard, J. S.; Luo, Y.; Armbrüster, M.; Meurig, T. J., Sir.; Midgley, P. A. Revealing the Atomic Structure of Intermetallic $GaPd_2$ Nanocatalysts by Using Aberration-Corrected Scanning Transmission Electron Microscopy. *ChemCatChem* **2013**, *5*, 2599−2609.

(11) Rameshan, C.; Stadlmayr, W.; Penner, S.; Lorenz, H.; Hävecker, M.; Blume, R.; Rocha, T.; Teschner, D.; Knop, A.; Schlögl, R.; Zemlyanov, D.; Memmel, N.; Klötzer, B. In-situ XPS Study of Methanol Reforming on PdGa Near-Surface Intermetallic Phases. *J. Catal.* **2012**, *290*, 126−137.

(12) Friedrich, M.; Penner, S.; Heggen, M.; Armbrüster, M. High CO_2 Selectivity in Methanol Steam Reforming through ZnPd/ZnO Teamwork. *Angew. Chemie Int. Ed.* **2013**, *52*, 4389−4392.

(13) Rameshan, C.; Stadlmayr, W.; Weilach, C.; Penner, S.; Lorenz, H.; Hävecker, M.; Blume, R.; Rocha, T.; Teschner, D.; Knop, A.; Schlögl, R.; Memmel.; Zemlyanov, D.; Memmel, N.; Rupprechter, G.; Klötzer, B. Subsurface-Controlled CO_2 Selectivity of PdZn Near-Surface Alloys in H_2 Generation by Methanol Steam Reforming. *Angew. Chem., Int. Ed.* **2010**, *49*, 3224−3227.

(14) Bayer, A.; Flechtner, K.; Denecke, R.; Steinrück, H. P.; Neyman, K. M.; Rösch, N. Electronic Properties of Thin Zn Layers on Pd(111) During Growth and Alloying. *Surf. Sci.* **2006**, *600*, 78−94.

(15) Gabasch, H.; Knop-Gericke, A.; Schlögl, R.; Penner, S.; Jenewein, B.; Hayek, K.; Klötzer, B. J. Zn Adsorption on Pd(111): ZnO and PdZn Alloy Formation. *Phys. Chem. B* **2006**, *110*, 11391−11398.

(16) Weirum, G.; Kratzer, M.; Koch, H. P.; Tamtögl, A.; Killmann, J.; Bako, I.; Winkler, A.; Surnev, S.; Netzer, F. P.; Schennach, R. Growth and Desorption Kinetics of Ultrathin Zn Layers on Pd(111). *J. Phys. Chem. C* **2009**, *113*, 9788−9796.

(17) Stadlmayr, W.; Penner, S.; Klötzer, B.; Memmel, N. Growth, Thermal Stability and Structure of Ultrathin Zn-Layers on Pd(111). *Surf. Sci.* **2009**, *603*, 251−255.

(18) Stadlmayr, W.; Rameshan, Ch.; Weilach, Ch.; Lorenz, H.; Hävecker, M.; Blume, R.; Rocha, T.; Teschner, D.; Knop-Gericke, A.; Zemlyanov, D.; Penner, S.; Schlögl, R.; Rupprechter, G.; Klötzer, B.; Memmel, N.. Temperature-Induced Modifications of PdZn Layers on Pd(111). *J. Phys. Chem. C* **2010**, *114*, 10850−10856.

(19) Stadlmayr, W.; Penner, S.; Klötzer, B.; Memmel, N. Growth and Alloying of Ultra-thin Zn Layers on Pd(110). *J. Phys. Chem. C* **2012**, *116*, 3635−3644.

(20) Fauster, Th. Surface Geometry Determination by Large-Angle Ion Scattering. *Vacuum* **1988**, *38*, 129−142.

(21) Rabalais, J. W. Principles and Applications of Ion Scattering Spectroscopy − Surface Chemical and Structural Analysis. *Wiley Interscience Series on Mass Spectroscopy*; Wiley: New York, 2003.

(22) Niehus, H.; Heiland, W.; Taglauer, E. Low-Energy Ion Scattering at Surfaces. *Surf. Sci. Rep.* **1993**, *17*, 213−303.

(23) The indexing of crystallographic directions used in the present work for Pd(111) differs from the one used in ref 17. Whereas in the latter work the (111) surface normal points towards the bulk, the present convention uses a (111) surface normal pointing towards vacuum. As a consequence the $[\bar{2}11]$ direction of the present work corresponds to the $[\bar{1}2\bar{1}]$ direction of ref 17.

(24) Detzel, Th.; Memmel, N.; Fauster, Th. Growth of Ultrathin Iron films on Copper(001): An Ion-Scattering Spectroscopy Study. *Surf. Sci.* **1993**, *293*, 227−238.

(25) Wannek, Ch.; Harbrecht, B. Phase Equilibria in the Palladium-Rich Part of the Gallium-Palladium System. The Crystal Structures of Ga_3Pd_7 and Ga_{1-x} Pd_{2+x}. *J. Alloys Compd.* **2001**, *316*, 99−106.

(26) Kovnir, K.; Schmidt, M.; Waurisch, C. H.; Armbrüster, M.; Prots, Y.; Grin, Y. Refinement of the Crystal Structure of Dipalladium Gallium, Pd_2Ga. *Z. Kristallogr. NCS* **2008**, *223*, 7−8.

(27) Bucher, J. P.; Hahn, E.; Fernandez, P.; Massobrio, C.; Kern, K. Transition from One- to Two-Dimensional Growth of Cu on Pd(110) Promoted by Cross-Exchange Migration. *Europhys. Lett.* **1994**, *27*, 473−478.

(28) Chen, Z. X.; Neyman, K. M.; Gordienko, A. B.; Rösch, N. *Phys. Rev. B* **2003**, *68*, 075417.

(29) Prinz, J.; Gaspari, R.; Pignedoli, C. A.; Vogt, J.; Gille, P.; Armbrüster, M.; Brune, H.; Gröning, O.; Passerone, D.; Widmer, R. Isolated Pd Sites on the Intermetallic PdGa(111) and PdGa (−1−1-1) Model Catalyst Surfaces. *Angew. Chem., Int. Ed.* **2012**, *51*, 9339−9343 From the data given in this reference, the cohesive energy per atom of PdGa is calculated as $E_{coh}^{PdGa} = 1/n\Delta H_f + 1/2E_{coh}^{Pd} + 1/2E_{coh}^{Ga}$, where $\Delta H_f = -5.46$ eV is the energy of formation per unit cell of bulk PdGa, n=8 is the number of atoms per PdGa unit cell, $E_{coh}^{Pd} = -3.69$ eV and $E_{coh}^{Ga} = -2.78$ eV are the cohesive energies of bulk Pd and Ga, respectively..

(30) A (100) surface orientation was erroneously suggested in ref 15. for the PdZn film as the oblique nature of the Pd(111) surface unit cell was not properly taken into account in the sequence of arguments. More likely, the observed diffraction pattern results from a coincidence structure between the substrate and a slightly skewed bulk-like PdZn alloy film, however with a (111) surface orientation [Stadlmayr, , W. Ph.D. Thesis; University of Innsbruck: Innsbruck, Austria, **2012**,].